Journal of Catalysis **212,** 33–38 (2002)
doi:10.1006/jcat.2002.3737

Promoter Sensitive Shapes of Co(Ni)MoS Nanocatalysts in Sulfo-Reductive Conditions

Hannes Schweiger,* Pascal Raybaud,*,[1] and Hervé Toulhoat†

*Division Chimie et Physico-chimie Appliquées, Département Thermodynamique et Modélisation Moléculaire, Institut Français du Pétrole, 1-4 av. de Bois-Préau, BP311, 92852 Rueil-Malmaison Cedex, France; and †Direction Scientifique, Institut Français du Pétrole, 1-4 av. de Bois-Préau, BP311, 92852 Rueil-Malmaison Cedex, France

Received May 27, 2002; revised June 27, 2002; accepted June 27, 2002

An innovative approach coupling DFT calculations and simple thermodynamics is developed for determining surface energies and morphologies of Co(Ni)MoS nanocatalysts used in hydrotreatment. According to sulfo-reductive conditions, three regimes are put forward. For high chemical potentials of sulfur, the promoter localization is found to be stable on both particle edges. Intermediate sulfiding conditions enhance the selective affinity of Co for the S edge only, whereas Ni remains stable on both edges. Finally, the destabilization of the mixed phases is found in highly reductive regimes.

Key Words: **hydrotreatment; Co(Ni)MoS catalyst; morphology; surface energy; density functional theory; scanning tunneling microscopy.**

1. INTRODUCTION

A better description of Co(Ni)MoS phases presents a huge interest for improving the preparation, activation, and usage of hydrotreating (HDT) catalysts for industrial refining (1, 2). Various characterization techniques such as Mössbauer spectroscopy (3), X-ray photoelectron spectroscopy (4, 5), extended X-ray absorption fine structure (EXAFS) (6–10), and more recently scanning tuneling microscopy (STM) (11, 12) have brought many insights into the nature and—to a certain extent—the local properties of the active phase. However, it is still difficult to identify physical features characteristic of the CoMoS or the NiMoS system, whereas it is well known that the two phases exhibit different activities and selectivities in HDT reactions, specifically concerning hydrodenitrogenation (13).

Since the early geometrical model proposed by Kasztelan *et al*. (14) and Toulhoat and Kasztelan (15), no attempt has been made to determine the morphologies of ternary systems, such as Co(Ni)MoS nanoparticles used in HDT, although it is mandatory to provide a precise inventory of surface sites. To solve this problem, surface energies must be evaluated under working conditions. To this end, there is still no straightforward experimental techniques, while DFT has recently allowed theoretical predictions for various systems (16–18).

Developing further our recent approach (17), we compare CoMoS, NiMoS, and MoS_2 active phases: we find shapes sensitive to the chemical potential of sulfur and to the nature of the promoter; CoMoS and NiMoS presenting distinct behaviours.

2. METHODS

All total energy calculations presented here are based on the plane wave density functional theory within the generalized gradient approximation (19). In a fully consistent way with those used and described in (17), we used the Vienna ab-initio simulation package to solve the Kohn–Sham equations (20) within the projected augmented wave formalism (21). All calculations were carried out with Γ-point sampling, taking into account the size of the cluster.

The edge energies of the Co(Ni)MoS particles, generically called M′MoS, were determined unambiguously by simulating triangular-shaped clusters, which already offered an elegant way to calculate surface energies for the nonpromoted metallic edge and S edge, respectively (17).

At thermodynamic equilibrium, the grand canonical potential, Ω, for the M′MoS nanoparticle of size n, can be expressed by

$$\Omega(n, \mu_S) = E_{M'MoS} - n_{Mo}^{tot} E_{MoS_2}^{ref} - \frac{n_{M'}^{tot}}{x} E_{M'_xS_y}^{ref} - n_S \mu_S, \quad [1]$$

where

$$n_S = 2n_{Mo}^{tot} + \frac{y}{x} n_{M'}^{tot} - n_S^{tot}, \quad [2]$$

$E_{M'MoS}$ stands for the total energy of the promoted M′MoS triangle, containing n_{Mo}^{tot} molybdenum atoms, $n_{M'}^{tot}$ promoter atoms, and n_S^{tot} sulfur atoms. $E_{MoS_2}^{ref}$ is the total energy of an infinite MoS_2 monolayer expressed per MoS_2 unit. $E_{M'_xS_y}$

[1] To whom correspondence should be addressed. E-mail: Pascal.Raybaud@ifp.fr.

0021-9517/02 $35.00

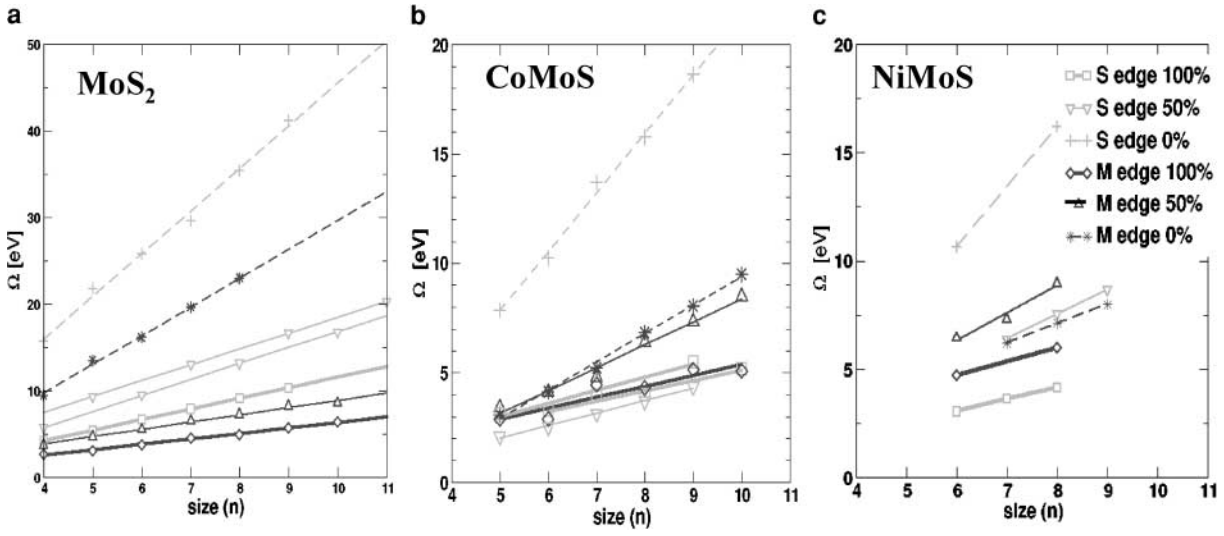

FIG. 1. Linear relationships obtained for Ω with respect to the cluster size according to Eq. [1] and $\mu_S = 0$: (a) nonpromoted phase (M = Mo) taken from (17), (b) Co promoted phase (M = Co), and (c) Ni promoted phase (M = Ni). The phases MoS_2, CoS_2, and Ni_3S_4 are used as references.

stands for the total energy of the stable phase M'_xS_y at a given μ_S. n_S stands for the excess (or lack) of sulfur atoms in the particle with respect to the stable monosulfide phases. The chemical potential of sulfur, μ_S, is related to sulfiding conditions (T, p_{H_2S}, and p_{H_2}) as explained in (17, 22).

The stability intervals for the Co and Ni sulfides used as reference phases (23) are defined as a function of μ_S by

$$\text{Co} \xrightarrow{-1.2\text{eV}} \text{Co}_9\text{S}_8 \xrightarrow{-0.02\text{eV}} \text{CoS}_2 \qquad [3]$$

and

$$\text{Ni} \xrightarrow{-1.1\text{eV}} \text{Ni}_3\text{S}_2 \xrightarrow{-0.5\text{eV}} \text{Ni}_3\text{S}_4. \qquad [4]$$

Equations [3] and [4] confirm that for traditional sulfo-reductive conditions, the Co_9S_8 and Ni_3S_2 phases are stable. For high (resp. low) μ_S, the pyrite CoS_2 (resp. Co *bcc*) phase as well as the Ni_3S_4 (resp. Ni *bcc*) has to be considered.

By differentiating the expression of Ω with respect to n, the edge energy derived from triangular shapes is given by

$$\sigma(\mu_S) = \sigma_0 - \mu_S \Delta n_S, \qquad [5]$$

where

$$\Delta n_S = \frac{n_S(n+1) - n_S(n)}{3}, \qquad [6]$$

and

$$\sigma_0 = \frac{\Omega(n+1,0) - \Omega(n,0)}{3}. \qquad [7]$$

Δn_S stands for the slope of the edge energy variation as a function of μ_S. As it was proven for nonpromoted systems, it is verified that Δn_S does not depend on the size of the promoted cluster. However, Δn_S depends on μ_S according to intervals defined by [3] and [4] and due to the changes in stoichiometry (y/x) of the M'_xS_y reference phases in Eq. [2]. Furthermore, it is crucial to verify that Ω varies linearly with respect to the cluster size to ensure the convergence of σ_0 values.

The diagrams shown in Fig. 1 demonstrate the good linear relationships between Ω and n, underpinning the reliability of our method for determining edge energies of ternary M′MoS particles. Triangular models used for M′MoS particles (containing up to 200 atoms) are similar to those of (17), but include the edge decoration with the promoter. Using the stable localizations found in (22), we simulate triangular-shaped particles by substituting edge Mo atoms by promoter atoms, M′. Assuming, for the present study, that the promoter content at the edge is kept fixed at 100%, three sulfur coverages around the edge are considered as those found in (16, 17, 22). The M′-edge (to be suppressed) contains 0% sulfur (resp. 50%, 100%), which means that each M′ promoter atom is bound to 4 (resp. 6, 6) sulfur atoms before relaxation. Symmetrically, the S edge contains 0% sulfur (resp. 50%, 100%), which means that each M′ atom is bound to 2 (resp. 4, 6) sulfur atoms per M′ atom. A more exhaustive choice of sulfur configurations were simulated in (16, 22) using periodic boundary conditions and revealed that the coverages retained for the present work are the most relevant coverages from an energetic point of view. Although we cannot exclude that some intermediate sulfur coverages might have been overlooked, these would have only a minor incidence on the final morphologies. Finally, the same criteria as those in (17) are applied for the geometry optimization (the first two layers of atoms counted from the edges inward are relaxed).

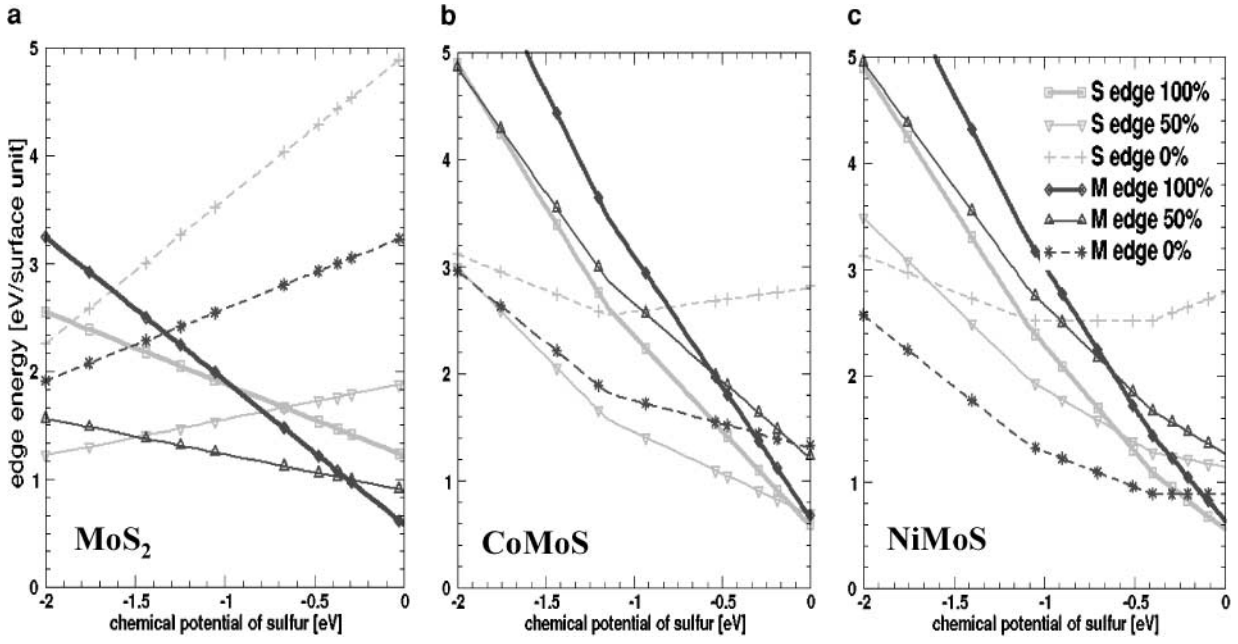

FIG. 2. Variation of edge energies as a function of chemical potential of sulfur: (a) nonpromoted phase (M = Mo) taken from (17), (b) Co promoted phase (M = Co), and (c) Ni promoted phase (M = Ni).

3. RESULTS AND DISCUSSION

Variations of edge energies, $\sigma(\mu_S)$, for nonpromoted and promoted phases, are shown in Fig. 2. Each line corresponds to one sulfur coverage. Slope changes are due to different reference states for the Co(Ni) sulfide phases, as explained in the previous section. Figures 3a–3c depict morphology diagrams deduced from the Gibbs–Curie–Wulff law (24) by taking into account the edge energy data from Figs. 2a–2c, respectively.

For high chemical potential of sulfur ($\mu_S \geq -0.25$ eV), surface energies of both promoted edges remain within a narrower window (0.6–1 eV) than those of the nonpromoted edges (0.6–1.4 eV). This is attributed to the levelling role of promoters on surface energies at high μ_S. Furthermore, in this region of high p_{H_2S}, Co or Ni promoters can be stabilized on both edges. Morphologies deduced from Figs. 3b and 3c for the Co or Ni promoted particles are close to hexagonal shapes. This result puts forward a major difference compared to the nonpromoted system whose shape was found to be close to a triangle, with the Mo edge only present in the same regime (see Fig. 3a and (17)). The analysis of the local structures shown in Figs. 4a and 4b, indicates that Co is found to be covered by 100% sulfur on both edges with six-fold coordination similar to that of Mo in the nonpromoted case. For Ni, the four-fold (resp. five-fold) environments on the S edge (resp. Mo edge) are preferred, due to strong edge reconstructions as shown by Fig. 4e (resp. Fig. 4c).

For the intermediate sulfiding regime ($-1.1 \leq \mu_S \leq -0.25$), the affinity of Co for the S edge is revealed. In this case, the S-edge energy becomes significantly lower than that of the Co edge (Fig. 2b), giving an unambiguous interpretation of the S-edge stabilization by Co as proposed in (25). However, as shown below, the local environments of Co are found to be rather different due to shortcomings of models used in (25) and effects of the chemical potential of sulfur. Furthermore, the most striking result is that the Ni-edge energy is found to be lower than that of the S edge (Fig. 2c); that is, the edge affinities are inverted in the CoMoS and NiMoS systems. As a first consequence, the stable domains for the promoter on the S edge are more restricted for Ni ($\mu_S \geq -0.75$ eV) than for Co ($\mu_S \geq -1.1$). Simultaneously, as the Ni-edge energy is significantly lower than the Co-edge energy, it cannot be excluded that Ni competes with Mo for the metallic edge as long as $\mu_S \geq -1$ eV. This situation is yet thermodynamically not possible for Co decorating preferentially the S edge. This explains why in Fig. 3c a large domain was found where Ni can be present on the metallic edge, whereas this domain does not exist for Co in Fig. 3b. Contrary to the nonpromoted particles, the morphology of the promoted systems reveals a growth of the metallic edge when μ_S is decreased. This trend is enhanced by Ni. The local environments were again different for CoMoS and NiMoS. On the one hand, Co exhibits a tetrahedral environment with 50% sulfur coverage on the S edge (similar to that of Fig. 4f). On the other hand, Ni is either in a square planar environment with 100% S on the S edge (Fig. 4e) or in a tetrahedral with 50% S (Fig. 4f), while it is exclusively in square planar on the Ni edge with 0% of sulfur (Fig. 4d). Confirming our previous periodic calculations (22), Co(Ni)-Mo (resp. Co(Ni)-S) distances are in

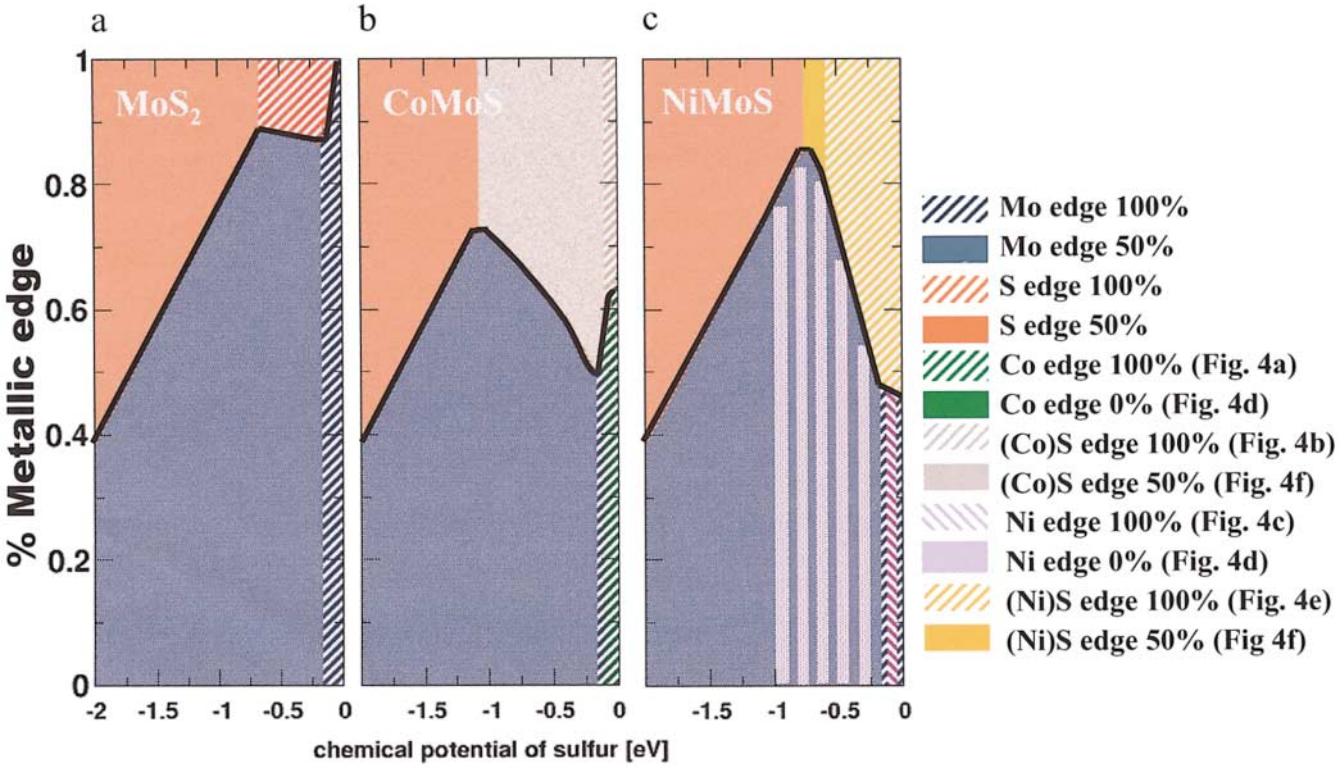

FIG. 3. Morphology and phase stability diagrams of the nanosized particles as a function of chemical potential of sulfur: (a) nonpromoted phase taken from (17), (b) Co promoted phase, and (c) Ni promoted phase. The thick black line indicates the equilibrium morphology. The ordinate represents the percentage of metallic edge exposed by the particle. For 100% (resp. 0%) M edge, the shape is a perfect Mo-edge (resp. S-edge) triangle. For 50% Mo edge, the shape is a perfect hexagon.

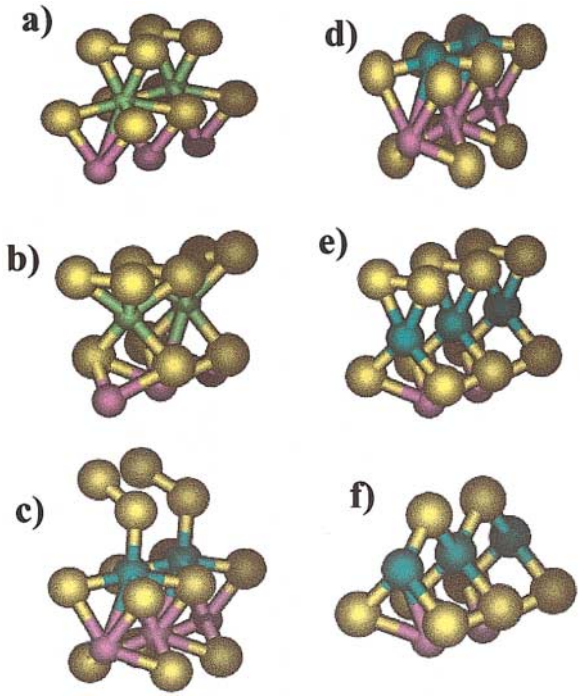

FIG. 4. Ball and stick representations of the local edge structures: (a) Co edge 100% S, (b) (Co)S edge 100% S, (c) Ni edge 100% S, (d) Ni edge 0% S, (e) (Ni)S edge 100% S, and (f) (Ni)S edge 50% S. (Sulfur: yellow, molybdenum: magenta, cobalt: light green, nickel: ultramarine blue).

good agreement with EXAFS data (6, 7): 2.76–2.95 Å (resp. 2.10–2.20 Å). As also observed by EXAFS (8), an increase of $\frac{p\mathrm{H_2}}{p\mathrm{H_2S}}$ implies a decrease of the sulfur coordination of the promoter.

An electronic interpretation of the inverted affinities can be proposed in terms of the filling of the acceptor d states located on the surface metal atoms, implying a decrease of the sulfur coverages of the slab edge in the order: MoS_2 > CoMoS > NiMoS > CuMoS (22). For nanosized particles under traditional sulfiding conditions, the MoS_2 particles exhibit 50% sulfur coverage on both edges, whereas CoMoS exhibits predominantly the S edge with 50% S coverage. The NiMoS phase predominantly exposes the Ni edge with 0% S coverage and a small fraction of S edge with 50% S. By increasing the $3d$-band filling according to the nature of the promoter, the latter's affinity changes from decorating the S edge to decorating the metallic edge.

To enrich the electronic characterizations of these systems, Fig. 5 shows STM images simulated for two stable CoMoS particles with Co located on the S edge. Figure 5a corresponds to $\mu_S \geq -0.25$ eV, where the promoted S-edge is covered by 100% sulfur. In Fig. 5b, the promoted S edge contains 50% sulfur, corresponding to lower μ_S values. In both cases, the metallic edge was terminated by Mo atoms with 50% sulfur. We observe that the bright rim deriving from electronic surface states localized

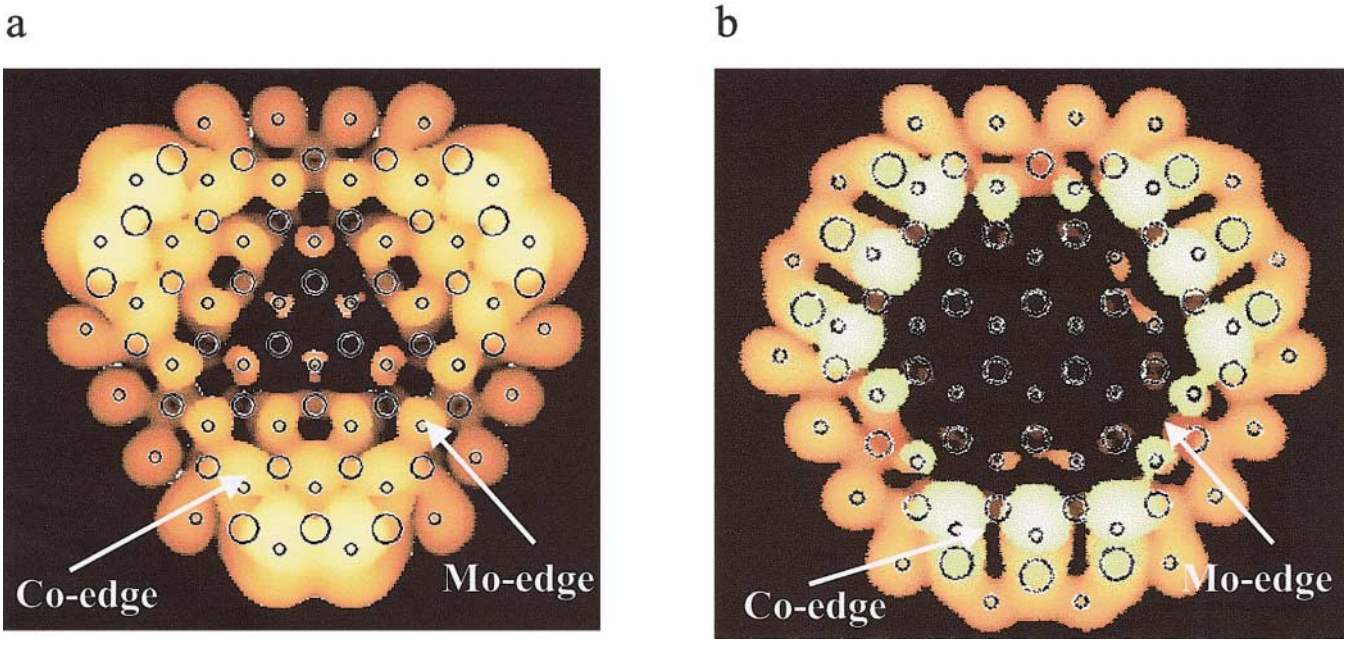

FIG. 5. STM images for two stable CoMoS clusters: (a) for $\mu_S \geq -0.25$, (b) for $-1.1 \leq \mu_S \leq -0.25$. The constant current STM topograph is simulated using the same approximations (26) and criteria as those described in (17). We increase the energy cut-off of 30% and sizes of the simulation box by 10 Å. (Small circles: S atom positions, medium circles: Mo atoms, large circle: Co atoms.)

on the second row of sulfur atoms bound to Co atoms is more intense than the rim observed at the Mo edge. This feature may qualitatively explain recent STM experiments (12) confirming that Co atoms are located at the S edge, in agreement with the above-described edge energy calculations.

Finally, it has to be underscored that an important third regime appears at highly reductive conditions ($\mu_S \leq -1.1$ eV) implying a complete destabilization of the mixed phase. This is due to the promoter's segregation into the more stable monosulfides Co_9S_8 (resp. Ni_3S_2) or metallic Co (resp. Ni) phases. To prevent from the loss of mixed phases, this highly reductive regime must be strictly avoided.

4. CONCLUSION

DFT calculations of edge energies for nanosized Co(Ni)MoS particles enabled us to distinguish three sulfiding regimes characterized by the chemical potential of sulfur. In the highly sulfiding regime ($\mu_S \geq -0.25$ eV), Co and Ni are stabilized on both edges. In the intermediate regime, i.e., traditional sulfiding conditions ($-1.1 \leq \mu_S \leq -0.25$ eV), the selective affinity of the promoters for one type of edge is revealed. In the highly reductive environment ($\mu_S \leq -1.1$ eV), the mixed phase becomes unstable. At the same time, we have demonstrated that the morphology is promoter sensitive. We think that the knowledge and the control of these three regimes are crucial for a better tuning of the catalyst activation at the sulfidation step. Our calculations predict that a mesoscopic property, such as the morphology, may be sensitive to local electronic properties. We have proposed a periodic trend which we expect to be confirmed by future calculations and experiments on M′MoS particles (M′ scanning the 3*d* row).

ACKNOWLEDGMENTS

This work was performed within the Groupement de Recherche Européen Dynamique Moléculaire Quantique Appliquée à la Catalyse, a joint project of the Conseil National de la Recherche Scientifique (CNRS), Institut Français du Pétrole (IFP), Universität Wien, Total Fina Elf, and Eindhoven University. The authors are grateful to Prof. J. Hafner and G. Kresse from the Universität Wien (CMS), and to their IFP colleagues: S. Kasztelan, V. Harlé, and T. Cseri for very fruitful scientific discussions.

REFERENCES

1. Topsøe, H., Clausen, B. S., and Massoth, F. E., *in* "Hydrotreating Catalysis and Science and Technology" (J. R. Anderson and M. Boudart, Eds.), Vol. 11. Springer-Verlag, Berlin/Heidelberg, 1996.
2. Prins, R., *in* "Handbook of Heterogeneous Catalysis" (G. Ertl, H. Knözinger, and J. Weitkam, Eds.), p. 1908. VHC, Verlagsgesellschaft/Weinheim, 1997.
3. Wivel, J., Candia, R., Clausen, B., Mørup, S., and Topsøe, H., *J. Catal.* **68**, 453 (1981).
4. Alstrup, I., Chorkendorff, I., Candia, R., Clausen, B. S., and Topsøe, H., *J. Catal.* **77**, 397 (1982).
5. Houssenbay, S., Kasztelan, S., Toulhoat, H., Bonnelle, J. P., and Grimblot, J., *J. Phys. Chem.* **93**, 7176 (1989).
6. Clausen, B. S., Topsøe, H., Candia, R., Villadsen, J., Lengeler, B., Als-Nielsen, J., and Christensen, F., *J. Phys. Chem.* **85**, 3868 (1981).
7. Bouwens, S. M. A. M., Prins, R., de Beer, V. H. J., and Koningsberger, D. C., *J. Phys. Chem.* **94**, 3711 (1990).

8. Bouwens, S. M. A. M., van Veen, J. A. R., Koningsberger, D. C., de Beer, V. H. J., and Prins, R., *J. Phys. Chem.* **95**, 123 (1991).
9. Calais, C., Matsubayashi, N., Geantet, C., Yoshimura, Y., Shinada, H., Nishijima, A., Lacroix, M., and Breysse, M., *J. Catal.* **174**, 130 (1998).
10. Shido, T., and Prins, R., *J. Phys. Chem.* **102**, 8426 (1998).
11. Helveg, S., Lauritsen, J. V., Lægsgaard, E., Stensgaard, I., Clausen, B. S., Topsøe, H., and Besenbacher, F., *Phys. Rev. Lett.* **84**, 951 (2000).
12. Lauritsen, J. V., Helveg, S., Lægsgaard, E., Stensgaard, I., Clausen, B. S., Topsøe, H., and Besenbacher, F., *J. Catal.* **197**, 1 (2001).
13. Prins, R., *Adv. Catal.* **46**, 399 (2002).
14. Kasztelan, S., Toulhoat, H., Grimblot, J., and Bonnelle, J., *Appl. Catal.* **13**, 127 (1984).
15. Toulhoat, H., and Kasztelan, S., "Proceedings, 9th International Congress on Catalysis, Calgary, 1988" (M. J. Phillips and M. Ternan, Eds.), Vol. 20–C3. Chem. Institute of Canada, Ottawa, 1988.
16. Raybaud, P., Hafner, J., Kresse, G., Kasztelan, S., and Toulhoat, H., *J. Catal.* **189**, 129 (2000).
17. Schweiger, H., Raybaud, P., Kresse, G., and Toulhoat, H., *J. Catal.* **207**, 76 (2002).
18. Raybaud, P., Digne, M., Iftimie, R., Wellens, W., Euzen, P., and Toulhoat, H., *J. Catal.* **201**, 236 (2001).
19. Perdew, J. P., and Wang, Y., *Phys. Rev. B* **45**, 13,244 (1992).
20. Kresse, G., and Furthmüller, J., *Comput. Mater. Sci.* **6**, 15 (1996).
21. Kresse, G., and Joubert, D., *Phys. Rev. B* **59**, 1758 (1999).
22. Raybaud, P., Hafner, J., Kresse, G., Kasztelan, S., and Toulhoat, H., *J. Catal.* **190**, 128 (2000).
23. Raybaud, P., Hafner, J., Kresse, G., and Toulhoat, H., *J. Phys. Condens. Matter* **9**, 11,085 (1997).
24. Wulff, G., *Z. Kristallogr.* **34**, 449 (1901).
25. Byskov, L. S., Norskov, J. K., Clausen, B. S., and Topsøe, H., *Catal. Lett.* **64**, 95 (2000).
26. Tersoff, J., and Hamann, D. R., *Phys. Rev. B* **31**, 805 (1985).